Testing atmospheric mixing sum rules at precision neutrino facilities

Peter Ballett,[1,*] Stephen F. King,[2,†] Christoph Luhn,[1,‡] Silvia Pascoli,[1,§] and Michael A. Schmidt[3,¶]

[1]IPPP, Department of Physics, Durham University, South Road, Durham DH1 3LE, United Kingdom
[2]School of Physics and Astronomy, University of Southampton, Highfield,
Southampton SO17 1BJ, United Kingdom
[3]ARC Centre of Excellence for Particle Physics at the Terascale, School of Physics,
The University of Melbourne, Victoria 3010, Australia

We study the prospects for testing classes of atmospheric mixing sum rules at precision neutrino facilities. Such sum rules, which correlate the atmospheric mixing angle θ_{23} with the recently measured reactor angle θ_{13} and the cosine of the oscillation phase δ, are predicted by a variety of semidirect models based on discrete family symmetry classified in terms of finite von Dyck groups. We perform a detailed simulation of the performance of the next generation of oscillation experiments, including the wideband superbeam and low-energy neutrino factory proposals, and compare their discriminating power for testing atmospheric mixing sum rules.

PACS numbers: 11.30.Hv, 14.60.Pq

I. INTRODUCTION

The recent measurement of the reactor mixing angle θ_{13}, by the Daya Bay [1] and RENO [2] experiments, completes the measurement of the mixing angles in the Pontecorvo-Maki-Nakagawa-Sakata (PMNS) matrix after the first hints which appeared in 2011 [3]. The reactor angle θ_{13} turns out to be sizable, $\sin^2(2\theta_{13}) = 0.089 \pm 0.010 \pm 0.005$ [1], close to the upper bound of the CHOOZ experiment [4]. This discovery has ruled out many of the most popular models of lepton flavor, which predicted small or even vanishing θ_{13} at leading order. Attention is now focused on models which can naturally incorporate the large value of θ_{13}. However, many such models do not predict this angle uniquely, but instead predict atmospheric mixing sum rules, where the deviation of the atmospheric angle from its maximal value is controlled by the product of the sine of the reactor angle and the cosine of the oscillation phase δ. The testability of these atmospheric mixing sum rules at future precision neutrino facilities forms the subject of the present paper.

At the time of writing, five parameters describing the neutrino sector have been measured: three mixing angles and two mass-squared differences. The magnitude of CP-violating effects in the lepton sector remains unknown, along with the sign of the largest mass-squared difference. One final degree of freedom is given by the absolute neutrino mass scale, which is bounded from above in the 1 eV region by the results of tritium beta decay experiments as well as cosmological and astrophysical

data [5]. The mixing angles and phases constitute the PMNS matrix, which describes the misalignment between flavor and mass bases. In the conventional parametrization, it is expressed by

$$
U_{\mathrm{PMNS}} = \begin{pmatrix} 1 & 0 & 0 \\ 0 & c_{23} & s_{23} \\ 0 & -s_{23} & c_{23} \end{pmatrix} \begin{pmatrix} c_{13} & 0 & s_{13}e^{-i\delta} \\ 0 & 1 & 0 \\ -s_{13}e^{-i\delta} & 0 & c_{13} \end{pmatrix}
$$
$$
\times \begin{pmatrix} c_{12} & s_{12} & 0 \\ -s_{12} & c_{12} & 0 \\ 0 & 0 & 1 \end{pmatrix} \begin{pmatrix} 1 & 0 & 0 \\ 0 & e^{i\frac{\alpha_{21}}{2}} & 0 \\ 0 & 0 & e^{i\frac{\alpha_{31}}{2}} \end{pmatrix},
$$

where $s_{ij} = \sin\theta_{ij}$, $c_{ij} = \cos\theta_{ij}$ and α_{ij} are the two possible Majorana phases. The current 3σ intervals for the parameters of the neutrino sector have been determined in a recent global analysis of oscillation data [6] to be

$$\theta_{12} = [31°, 36°], \qquad \theta_{13} = [7.2°, 10°], \qquad \theta_{23} = [36°, 55°],$$
$$\Delta m_{21}^2 = [7.00, 8.09] \times 10^{-5}\mathrm{eV}^2,$$
$$\Delta m_{31}^2 = [2.27, 2.70] \times 10^{-3}~\mathrm{eV}^2 \quad (\mathrm{NO}),$$
$$\Delta m_{32}^2 = [-2.65, -2.24] \times 10^{-3}~\mathrm{eV}^2 \quad (\mathrm{IO}),$$

with NO and IO denoting normal and inverted neutrino mass ordering.[1] The phase δ, which enters the oscillation formulas through subdominant terms, is currently unconstrained at 3σ. The Majorana phases are also unconstrained, but, as they do not enter the neutrino oscillation formulas, they must be addressed by alternative experiments.

*peter.ballett@durham.ac.uk
†s.f.king@soton.ac.uk
‡christoph.luhn@durham.ac.uk
§silvia.pascoli@durham.ac.uk
¶michael.schmidt@unimelb.edu.au

---

[1]For similar but independent global fits to neutrino oscillation data, see [7].

The large atmospheric and solar mixing angles evident in the leptonic sector have motivated a number of authors to consider the existence of an underlying (discrete) symmetry which connects states of different flavor. Approaches of this type typically generate first-order expressions for the PMNS matrix which are populated by simple algebraic values, and a number of such patterns have been proposed, see Ref. [8] for reviews with extensive lists of references. The simplest mixing patterns of this kind involve maximal atmospheric mixing and a zero reactor angle differing only in the solar mixing angle θ_{12}. For example the tribimaximal (TB) mixing matrix [9]

$$U_{\text{TB}} = \begin{pmatrix} \sqrt{\frac{2}{3}} & \frac{1}{\sqrt{3}} & 0 \\ -\frac{1}{\sqrt{6}} & \frac{1}{\sqrt{3}} & \frac{1}{\sqrt{2}} \\ \frac{1}{\sqrt{6}} & -\frac{1}{\sqrt{3}} & \frac{1}{\sqrt{2}} \end{pmatrix} P \qquad (1)$$

predicted $\sin \theta_{12} = 1/\sqrt{3}$. Another example referred to as golden ratio (GR) mixing is given by the following matrix [10]:

$$U_{\text{GR}} = \begin{pmatrix} \cos \vartheta & \sin \vartheta & 0 \\ -\frac{1}{\sqrt{2}} \sin \vartheta & \frac{1}{\sqrt{2}} \cos \vartheta & \frac{1}{\sqrt{2}} \\ \frac{1}{\sqrt{2}} \sin \vartheta & -\frac{1}{\sqrt{2}} \cos \vartheta & \frac{1}{\sqrt{2}} \end{pmatrix} P, \qquad (2)$$

where $\tan \vartheta = 1/\phi$, with ϕ given by the golden ratio $(1 + \sqrt{5})/2$. Although these are both excluded by the observation of the reactor angle, the first or second columns of these matrices may be preserved in the presence of a nonzero reactor angle, as we now discuss.

In the framework of so-called "direct models," both the mixing patterns above have been shown to arise from some discrete family symmetry group G_f (for example A_4, S_4 or A_5) [8]. These are small finite groups with three-dimensional representations, and frequently, the three generations of leptonic SU(2) doublets are assigned to a triplet representation ensuring that their mixing is highly constrained. New scalar fields are then introduced, called flavons, which are also assigned to representations of G_f, but are typically neutral under the standard model gauge group. The Lagrangian can then be written down in the conventional fashion, with all terms included that are consistent with the symmetries of the theory. The terms which constitute the flavon-flavon interactions are referred to as the flavon potential; in successful models the minimum of this potential will require nonzero vacuum expectation values (VEVs) for a subset of the flavon fields, a feature which will spontaneously break G_f. The PMNS mixing matrix then results from the presence of residual symmetries.

The residual symmetry in the charged lepton sector is based on the generator T, while that in the (Majorana) neutrino sector is called the Klein symmetry based on the Z_2 generators S and U, where all three generators are contained inside G_f in the "direct" models [8,11]. In order to switch on the reactor angle, a popular approach is to break only the U generator, leading to the so-called "semidirect" approach [8] where the surviving S generator maintains a particular column of the original mixing matrix. This keeps the solar angle close to its desired value, while allowing a nonzero reactor angle which is correlated with the deviations of the atmospheric angle from its maximal value, depending on the cosine of the oscillation phase.

In this work, we focus on the experimental prospects of constraining generalized versions of such correlations known as atmospheric mixing sum rules: relations between the atmospheric mixing angle θ_{23} and the recently measured reactor angle θ_{13}. We shall show that these can describe a wide range of semidirect models in the literature and, with the increased sensitivity of the next generation of oscillation experiments, will be significantly constrained for the first time over the next few decades. After a study of the compatibility of different sum rules with the current experimental results, as well as the projected sensitivity of the extant experimental program, we study two different experimental proposals explicitly, namely a wideband superbeam (WBB) with a long baseline of around 2300 km as well as the low-energy neutrino factory (LENF).

Although focusing on atmospheric mixing sum rules, this work will also be relevant to the study of other types of correlations which are associated with models of flavor. For example, solar mixing sum rules, which connect θ_{12} to θ_{13} and $\cos \delta$ [12], can be associated with models of discrete symmetries where the leading-order mixing pattern receives corrections from the charged lepton sector. The ability to constrain these sum rules relies on the attainable precision on θ_{12}, and this will be set by the future medium-baseline reactor experiments, JUNO and RENO-50, which predict an accuracy of below 1% [13]. However, to constrain $\cos \delta$, the precision of the long-baseline physics program, as considered in this work, will be essential.

The paper is organized as follows. In Sec. II, we discuss the sum rules arising in different classes of models. Technical group theoretical details are deferred to the Appendix. Section III addresses the validity of the linearization approximation. The current experimental constraints on the sum rules and the projected sensitivity of the current experimental program are discussed in Sec. IV, while prospects of next-generation experiments are presented in Sec. V. Finally, we make our concluding remarks in Sec. VI.

II. DISCRETE FAMILY SYMMETRIES AND SUM RULES

In general, the incorporation of discrete family symmetries into any extension of the standard model can only further our understanding of flavor if it manages to reduce the number of free parameters in the theory. It is, therefore, generally expected for these models to generate correlations amongst the physical parameters governing the

leptonic Yukawa sector. For a given model based on discrete family symmetries, the correlations between the PMNS matrix elements will, in general, correspond to a nonlinear relation amongst the mixing angles and phases.

It is convenient to parametrize these relations by employing the notation of Ref. [14], which introduces the parameters s, r and a defined by

$$\sin\theta_{12} \equiv \frac{1+s}{\sqrt{3}}, \qquad \sin\theta_{13} \equiv \frac{r}{\sqrt{2}}, \qquad \sin\theta_{23} \equiv \frac{1+a}{\sqrt{2}}.$$

These parameters, which describe the deviations from tribimaximality, provide a close phenomenological fit to the known mixing angles. The recent global fit in Ref. [6] provides the following 1σ intervals (for normal neutrino mass ordering)

$$-0.07 \leq s \leq -0.02, 0.20 \leq r \leq 0.23, -0.12 \leq a \leq -0.05.$$

In this paper, we will focus on a specific set of correlations which are primarily dependent on the atmospheric mixing angle θ_{23}, the reactor mixing angle θ_{13} and the cosine of the Dirac CP phase, $\cos\delta$. It will be useful to work with the first-order expansion of the exact relation in the small parameters s, r and a, which we call the sum rule. For the models that we are interested in, these will take the general form

$$a = a_0 + \lambda r \cos\delta + \mathcal{O}(r^2, a^2), \tag{3}$$

where we will treat a_0 and λ as new model-dependent constants. As the mixing angles have already been measured, the sum rule can be used to predict the Dirac CP phase δ. For phenomenologically viable models, a_0 will always be small, of order of the s parameter, and in the analysis of Sec. V it will be largely neglected. A discussion of higher-order effects correcting the sum rule is presented in Sec. IV.

Although we will consider questions based on a range of values of λ, there are two values which we would like to highlight. These two choices have a degree of universality having arisen in the literature from fully consistent models, while also remaining the only simple rules that we have found in our more phenomenological treatments: the first of these rules has $\lambda = 1$, and the second is given by $\lambda = -1/2$. We will now illustrate this discussion with a few examples from the literature which will highlight these two important cases. A recent model presented in Ref. [15] imposes an A_4 symmetry broken spontaneously by a set of flavons, which leads to the second column of the PMNS mixing matrix fixed at its tribimaximal value (for other models which lead to this prediction, see Ref. [16]),

$$|U_{e2}| = |U_{\mu2}| = |U_{\tau2}| = \frac{1}{\sqrt{3}}.$$

The corresponding exact relation can be linearized in terms of the s, r and a parameters [14],

$$a = -\frac{r}{2} \cos\delta, \tag{4}$$

which is a specific realization of our general rule, Eq. (3) with $a_0 = 0$ and $\lambda = -1/2$. A different sum rule has been found in Ref. [17], once again by spontaneously breaking the group A_4; however, in this model the first column of the PMNS matrix is fixed at its tribimaximal value (see Ref. [18] for alternative models with this prediction). This imposes the relations,

$$|U_{e1}| = \sqrt{\frac{2}{3}} \quad \text{and} \quad |U_{\mu1}| = |U_{\tau1}| = \frac{1}{\sqrt{6}}.$$

Using these relations to compute the sum rule, one finds [17],

$$a = r \cos\delta, \tag{5}$$

which corresponds to $a_0 = 0$ and $\lambda = 1$.

A novel method was recently introduced by Hernandez and Smirnov in Ref. [19] which produces flavor-symmetric correlations amongst the PMNS mixing matrix elements, while making minimal assumptions about the details of the model. This approach was built around the assumption that there exists a discrete flavor group which is broken spontaneously into two subgroups. These subgroups act independently on the charged lepton and neutrino sectors of the theory, and their misalignment leads to a nontrivial PMNS matrix. If we assume, in this framework, that some of the known symmetries of the leptonic mass terms are in fact residual symmetries arising from this larger broken group, constraints can be placed on the PMNS matrix in a general manner, regardless of the precise implementation of the symmetry breaking. For the groups that we will focus on, the constraints which arise from this construction fix one column of the PMNS matrix:

$$|U_{\alpha i}|^2 = \eta \quad \text{and} \quad |U_{\beta i}|^2 = |U_{\gamma i}|^2 = \frac{1-\eta}{2},$$

where $\{\alpha, \beta, \gamma\} = \{e, \mu, \tau\}$ and the parameter η is a model-dependent constant, which can be found in the Appendix. Fixing a column of the PMNS matrix introduces two independent constraints on the mixing angles. For the cases that we are interested in, either the first or second column is fixed, and we can express these constraints as an exact prediction for s as a function of r^2, and an atmospheric sum rule of the general form as given in Eq. (3). For further discussion on the phenomenological ramifications of a single fixed symmetric column (or row) in the PMNS matrix, see Ref. [20].

One can show that, working within this framework, there is a finite number of possible values for η, depending on the underlying group and the choice of generators preserved after spontaneous symmetry breaking. Using the exact expressions for s, we can make predictions for each choice of η and exclude any models that are incompatible with the current experimental data. At the end of this process, we are left with a finite number of models with phenomenologically viable predictions of s and a definite atmospheric sum rule. It turns out that these are all closely related to the two special sum rules that we have already identified in Eqs. (4) and (5). Generally they predict sum rules with values of λ numerically close to 1 or $-1/2$. A full listing of these rules is given in Table I, and we refer the reader to the Appendix for the details of their derivation. We see that by choosing different residual generators, we find eight distinct sum rules of the type of Eq. (3) which are compatible with the current phenomenological data.

A number of the scenarios that we have identified in Table I can be explained in terms of the TB and GR matrices given in Eqs. (1) and (2). The three scenarios based on an A_4 symmetry all lead to a value of the second column of the PMNS matrix fixed at its tribimaximal value; similarly, the S_4 scenario with the generator choice $T_e - S_1$ fixes the prediction of the first column to be tribimaximal. The scenario based on A_5 with unbroken generators $T_e - S_1$ $(T_e - S_2)$ fixes the first (second) column of the PMNS matrix to the equivalent values of the GR mixing matrix.

TABLE I.   The phenomenologically viable sum rules of the form $a = a_0 + \lambda r \cos \delta$ (where a, r are the atmospheric and reactor angle deviations from tribimaximal mixing and δ is the CP-violating oscillation phase) arising in the Hernandez-Smirnov framework for finite von Dyck groups. In this table, m gives the order of the generator which controls the charged lepton mass matrix, $T_\alpha^m = 1$, while S_i is the generator of the von Dyck group that is identified with one of the generators of the Klein symmetry of the neutrino mass matrix (with the other Klein symmetry generator being unrelated to the von Dyck group, as in so-called semidirect models). Analytical expressions for the solar angle deviation from tribimaximal mixing s and the constants a_0 and λ are given in Table II. The numerical values are obtained for the current best-fit value of $\sin^2 2\theta_{13} = 0.089$ [1].

G_f	m	T_α, S_i	s	a_0	λ
	3	T_e, S_2	0.012	0	-0.5
A_4	3	T_μ, S_2	0.012	0	-0.5
	3	T_τ, S_2	0.012	0	-0.5
	3	T_e, S_1	-0.024	0	1
S_4	4	T_μ, S_2	-0.124	-0.167	-0.408
	4	T_τ, S_2	-0.124	0.167	-0.408
	5	T_e, S_1	-0.118	0	1.144
A_5	5	T_e, S_2	-0.079	0	-0.437
	5	T_μ, S_2	0.054	0.067	-0.532
	5	T_τ, S_2	0.054	-0.067	-0.532

III. VALIDITY OF LINEARIZATION

In general, the correlations predicted by flavor-symmetric models are nonlinear relations between the oscillation parameters. We have discussed how the form of these correlations simplifies when only the first-order terms in the parameters s, r and a are retained, and we will now address the impact of higher-order terms. We consider the model presented in Ref. [17], which fixes the elements of the first column of the PMNS matrix to their tribimaximal values. As a function of r and a, this model predicts that $\cos \delta$ is given by the composition of the following functions:

$$\cos \delta = \frac{(-2 \sin^2 \theta_{12} + \cos^2 \theta_{12} r^2) \cos(2\theta_{23})}{\sqrt{2} r \sin(2\theta_{12}) \sin(2\theta_{23})},$$

$$\cos \theta_{12} = \frac{2}{\sqrt{3(2 - r^2)}}, \quad \text{and} \quad \sin \theta_{23} = \frac{1 + a}{\sqrt{2}}.$$

When linearized, these relations lead to the simpler expression $\cos \delta = a/r$. In Fig. 1 we have computed the predictions of $\cos \delta$ as a function of a for both the exact relation and the sum rule, with r varied within its experimentally allowed 3σ region. We see that for this model the difference between the two treatments is small. The impact of higher-order corrections can only be assessed on a case-by-case basis once the exact correlations are known; however, due to the smallness of the r and a parameters, we expect the linear approximation to be a good one. This is confirmed by our simulations for the known exact correlations, and therefore we will focus our later analysis on the linearized relations. This also allows us to treat the universality that we have observed in Sec. II: all viable sum rules that we have identified are either close to $\lambda = 1$ or $\lambda = -1/2$.
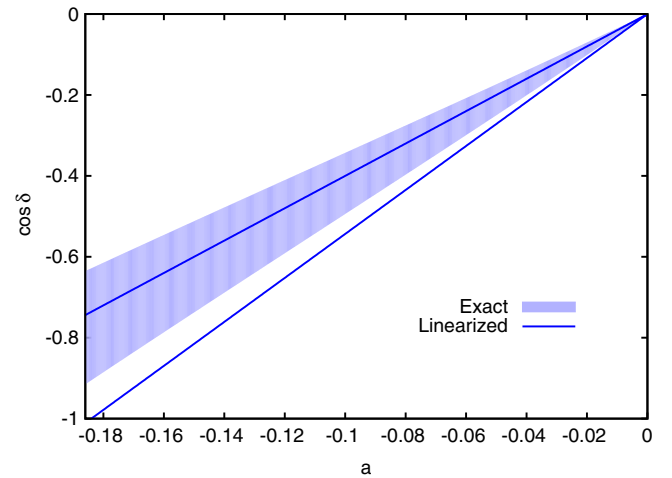

FIG. 1 (color online).   A comparison between the exact correlation and the sum rule for the model presented in Ref. [17], which fixes the elements of the first column of the PMNS matrix to their tribimaximal values. The solid (empty) region denotes the exact (linearized) prediction for $\cos \delta$ which is produced by varying r over its current 3σ allowed interval.

For the classes of phenomenologically viable models that we have found, the differences between similar sum rules are small and will be very challenging to measure.

IV. COMPATIBILITY OF SUM RULES WITH EXISTING AND PROJECTED DATA

The global neutrino oscillation data already constrain models which exhibit discrete flavor symmetries. For a given model, our general sum rule can be used to predict the value $\cos \delta$. Fixing a, we define $\cos \delta$ by the mapping from r which is found by inverting Eq. (3); r is then allowed to vary across its 1σ interval [6] and the image of this mapping is taken to be the range of potential values for $\cos \delta$.

In Fig. 2 we show the predictions of our two specific sum rules and their compatibility with the current global data on a (the grey regions). We have also shown (the red bands) the projected sensitivity to the a parameter as reported in Ref. [21]. These projections are for the global parameter sensitivity in 2025 assuming only the current experimental program: five years of data from T2K, six from NOνA, and three years each for Double Chooz, RENO and Daya Bay. As we cannot predict the future best-fit value, the horizontal location of the predicted regions is largely irrelevant, and in Fig. 2 they have been arbitrarily centred around the current best-fit value.

We see that the predictions of δ for these two models are currently consistent with the global data. However, the overlap for some of these 1σ intervals can be seen to require some quite specific correlations: for example, $\lambda = -0.5$ and NO requires $\cos \delta \gtrsim 0.5$. With the projected sensitivity to a, these correlations could create tension with the future data, and the consistency of these models will start to become rather constrained. For example, in a strictly CP-conserving theory, $\sin \delta$ must vanish. The corresponding value of $\cos \delta$ would then be difficult to reconcile with the sum rule given by $\lambda = 1$, leading to a possible exclusion of such a sum rule. The limiting factor for the general exclusion of these models with the current experimental program will be the attainable precision on $\cos \delta$. It has been shown that, in the most optimistic case, the current experimental program will only be able to provide a 3σ region for δ with a width of around 300° [22]. It is clear, therefore, that testing mixing sum rules will be a task to be addressed by a next-generation neutrino oscillation facility, one which focuses on precision.

V. TESTING SUM RULES AT NEXT-GENERATION FACILITIES

With the knowledge of the value of θ_{13} the campaign for a next-generation facility designed to make precision measurements of the neutrino mixing parameters is greatly strengthened. It is likely that within the extant experimental neutrino physics program, we will see hints towards the measurement of two of the most important unknowns in the conventional neutrino flavor-mixing paradigm: the sign of the atmospheric mass-squared difference and the value of the CP-violating phase, δ. It is, however, unlikely that these questions will be resolved at an acceptable statistical confidence level: the projected 3σ CP-violation discovery fraction with the current experimental program only reaches around 20% of the parameter space [21] and it is only modestly higher for the determination of the mass ordering at around 40%. The desire for a definitive 5σ answer to these questions provides the first motivation for the construction of a next-generation neutrino oscillation facility, capable of precision measurements of the

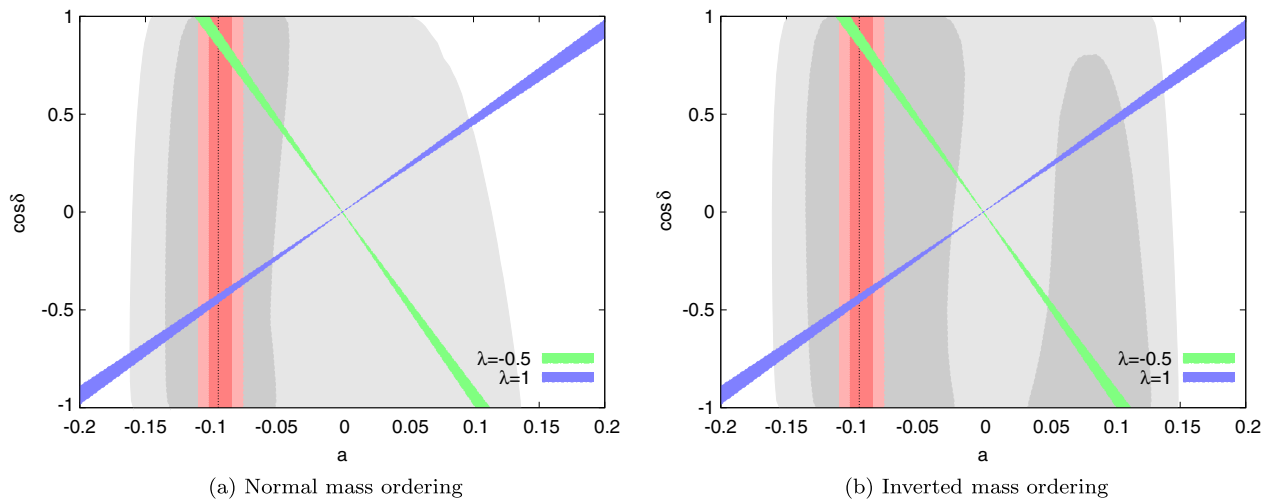(a) Normal mass ordering   (b) Inverted mass ordering

FIG. 2 (color online). The current experimental status of the sum rules in Eq. (3) given by $\lambda = 1$ and $\lambda = -0.5$, with $a_0 = 0$. The diagonal lines show the regions predicted for a and $\cos \delta$ given the 3σ bounds on r, assuming both (a) normal ordering and (b) inverted ordering. The vertical line shows the current best fit for a where the projected sensitivity is indicated by the red bands; the dark (light) grey regions show the current 1σ (2σ) allowed intervals [6].

oscillation parameters. In this work, we will focus on two such designs: the low-energy neutrino factory (LENF) and a wideband superbeam (WBB).

The WBB is an extrapolation of existing technology using a more powerful version of the conventional neutrino beam production method. Protons are accelerated towards a target, and the subsequent collision generates, amongst other things, pions and kaons. Magnetic horns then focus the meson beam, selecting π^+, the decay of which generates the neutrino beam, predominantly composed of ν_μ with a small contamination of ν_e, $\bar\nu_\mu$ and $\bar\nu_e$ which constitute a background to the signal, with an analogous composition for the initial selection of π^-. After years of experimental work on similar designs, this technology is very well understood and considerable expertise is to be found in the community. With a large value of θ_{13}, such a next-generation superbeam has been shown [23,24] to provide a quite competitive physics reach compared to other designs, and for a significant fraction of parameter space, may be sensitive to CP violation originating from the PMNS matrix. There are a number of proposed experiments based on the WBB design. The CERN to Pyhäsalmi superbeam has been developed, and recently recommended, by the LAGUNA-LBNO design study [25]. For this experiment neutrinos produced at CERN are detected by a 70 kton liquid argon detector (LAr) after a propagation distance of 2300 km at Phyäsalmi in Finland. There is a similar proposal for an intense long-baseline superbeam known as LBNE, which is based in America. In its first phase, the facility consists of a 10 kton liquid argon detector based on the surface at Homestake, separated by a distance of 1300 km from Fermilab. This should be viewed as the first step in a staged program, ultimately aiming for an underground detector of order 35 kton, which has been shown to have strong discovery potential for the mass ordering and CP-violation effects.

At a neutrino factory [26], a neutrino beam is produced via the decay of muons held in a storage ring. This process is very well understood and controlled, which leads to small systematic uncertainties and ultimately strong sensitivity to the neutrino mixing parameters. The typical design has evolved over the last few years. The original designs worked with a high-energy facility, with stored-muon energies of around 25 GeV [27]. This was shown to have exceptional sensitivity for small values of θ_{13}, down to $\sin^2 2\theta_{13} = 10^{-5}$ [28]. However, with the discovery of the large value of θ_{13} by the Daya Bay [1] and RENO [2] experiments, the consensus has now fallen on the low-energy variant, the LENF [29] designed with a stored-muon energy of around 10 GeV. At the LENF, a strong sensitivity to the PMNS parameters is achieved by focusing on the rich oscillation signal which can be found in the low-energy parts of the neutrino spectrum, a technique which relies on the enhanced number of events associated with larger values of θ_{13}. Optimization work on the LENF has shown it to be a versatile design [30,31] and a

strong candidate for a precision neutrino oscillation facility [32]. Assuming μ^- (μ^+) in the storage ring, the beam of a neutrino factory consists of ν_μ ($\bar\nu_\mu$) and $\bar\nu_e$ (ν_e). The LENF is designed to focus primarily on the measurement of "wrong-sign muons," the antiparticles of those in the storage ring, which are produced by charged-current interactions in the detector after the flavor transition $\bar\nu_e(\nu_e) \to \bar\nu_\mu(\nu_\mu)$. In addition to this "golden channel," it may also be possible to include the "platinum channel," observing electrons at the detector produced by incident $\bar\nu_e(\nu_e)$ [30]. This additional channel is only available to certain detector technologies, and has been shown to confer only a slight improvement for the traditional discovery searches; however, its impact on precision measurements is as yet unknown. Nevertheless, in this study we will not consider the impact of the platinum channel, only assuming the observation of μ^+ (μ^-) at the detector.

A number of alternative detector options are often considered for the LENF [28,30,31]. In this work, we are not looking to make a detailed comparison of designs, but instead to show the feasibility of constraining sum rules at next-generation facilities. As such, we have restricted our attention to two variants of the LENF detector design: a magnetized iron neutrino detector (MIND) and a magnetized liquid argon detector (mLAr) based on liquid argon time-projection chamber technology. These two technologies provide us with a fair estimate of performance of the current proposals (MIND), as well as a more optimistic assessment (mLAr) of the potential of a LENF. A LENF with a MIND has become the favored design of the International Design Study for a Neutrino Factory [33]. The MIND is composed of alternating sheets of iron and scintillator placed inside in a 1.5 T toroidal magnetic field. This technology is very well understood, based on an extrapolation of the MINOS detector to a larger scale, and has been the object of extensive study demonstrating strong physics reach [28,32,34,35]. A large magnetized liquid argon detector would be an ultimate detector for a LENF, as it allows for detailed event reconstruction, a low threshold energy and excellent energy resolution. Such a facility, and in particular the magnetization of the large detector volume, poses some technical challenges. In our study, we simulate a scenario based on a 50 kton mLAr which should be viewed as providing an optimistic upper bound on the performance of the LENF.

We have used the GLoBES package [36] to perform our simulations of the LENF and WBB experiments. Our model of the WBB design is based on Ref. [32], and assumes 10^{21} protons on target per year at 50 GeV, a baseline distance of 2300 km and a 70 kton (35 kton) liquid argon detector similar to the GLACIER [37] design. The fluxes for this setup are taken from Ref. [38] (for discussion see Ref. [39]). We have assumed a 90% detection efficiency and the backgrounds are taken as arising from a combination of the contamination of the beam and 0.5% of

neutral-current events at the detector. The detector has a low-energy threshold of 100 MeV with an energy resolution taken to be a flat 150 MeV for electrons and 200 MeV $\times \sqrt{E/\mathrm{GeV}}$ for muons. An error of 5% has been imposed on the signal and background, and a 2% uncertainty on the matter density. All of our simulations of the LENF design assume 10^{22} total useful muon decays divided equally between μ^- and μ^+. The LENF operates with a stored-muon energy of 10 GeV and a baseline distance of 2000 km. These have been shown to be near optimal choices for large θ_{13} [28,40,31]. Similar parameter choices have recently been recommended by the EUROnu Design Study [41], and coincide with the expected specifications of the International Design Study for the Neutrino Factory [42]. The assumptions in our model of the MIND have been kindly provided by P. Soler and R. Bayes and are based on ongoing work evolving from the proposals of Ref. [27], which has been recently reviewed in Ref. [43]. This model uses migration matrices to simulate both the appearance and disappearance channels, and considers backgrounds of charge misidentification, neutral current events and tau contamination. In our model of the mLAr, we have assumed a threshold energy of 0.5 GeV and a detection efficiency of 73% at the lowest energies, rising to 94% at 1 GeV. The energy resolution is a flat 10% and the background to the golden channel is taken as 0.1% of the incident right-sign muons, which models instances of charge misidentification, and 0.1% of the neutral-current events. We have imposed a 2% systematic uncertainty on both the signal and backgrounds, and a 2% uncertainty on the matter density.

The background to the appearance signals caused by ν_τ particles incident on the detectors, which produce electrons and muons by τ decay, is known as τ contamination [44,45]. It is known that this background affects the attainable sensitivity to the oscillation parameters, causing significant systematic shifts if not properly taken into account [46]. The degree with which an experiment can control the τ background differs by design. At the LENF, the dominant τ particles are right sign, and only significantly impact the disappearance channel measurements. Under the assumption that $\cos\delta$ will introduce the dominant uncertainty in the measurement of sum rules, we can conclude that the impact of τ contamination should be slight. For the WBB, the τ contamination will affect both appearance and disappearance channels. However, the greater kinematic information attainable with LAr detectors can significantly reduce the impact of this background: a cut-based analysis on transverse momentum is very effective at removing leptons originating from τ decay [47]. Therefore, to fairly implement the τ-contamination effect, we must use information from the experimental groups working on these detectors. This information is not available for LAr detectors, and we have chosen to omit the τ background at all of the facilities when we are making a

direct comparison of performance. The full implementation of τ contamination is possible for the LENF with MIND, and we have checked that there is no significant impact on our conclusions.

A. Precision for a, r and $\cos\delta$

We start our study by computing the precision with which the next-generation facilities can individually measure the parameters a, r and $\cos\delta$. An understanding of this precision should give us an indication of the potential precision towards generic sum rules in these variables, and help us to identify the dominant uncertainties and functional dependence of such a measurement. In the following analysis, we will refer to the parameter values which are used to generate the simulated data as the true values and the parameters which are extracted by fitting our models to the data as the fitted values. When necessary, true and fitted values will be distinguished by subscripts i.e. a_T and a_F. For each parameter of interest, we have scanned over a range of true values and then computed the allowed region (at 1, 3 and 5σ) in the fitted value of this parameter for both experimental setups, each with two different detector options. We marginalize over all of the otherwise unspecified oscillation parameters in each case. The allowed regions are then expressed as a function of the true parameter value and the difference between the fitted and true values.

The leftmost column in Fig. 3 shows the sensitivity to a for both the LENF (bottom row, solid lines for MIND and shaded regions for 50 kton magnetized LAr) and the WBB (top row, solid lines for 35 kton and shaded regions for 70 kton detectors). For large values of a_T, we find the magnitude of $\Delta a \equiv a_\mathrm{F} - a_\mathrm{T}$ to be between 0.005 and 0.015 at 3σ for the LENF, while the WBB has worse performance with a range of between 0.014 and 0.021. The attainable precision worsens notably for both experiments around $|a_\mathrm{T}| \lesssim 0.05$, where Δa can become potentially as high as 0.041 (0.089) for the LENF with magnetized LAr (MIND) and 0.117 (0.210) for the WBB with 35 kton (70 kton) LAr. This increase is due to the presence of a degeneracy. For a given value of a_T, we get two reasonably good solutions for the fit $a_\mathrm{F} \approx \pm a_\mathrm{T}$: a manifestation of the θ_{23} octant degeneracy [48]. This is not an exact degeneracy of the three-neutrino oscillation probability, and the ambiguity only appears for the smallest deviations from θ_{23} maximality. For all values of a_T, WBB performs worse than the LENF, and for both facilities, the optimistic detectors perform better than the more conservative ones. However, if we focus on the best-fit values for a given by recent global fits, at around $a = -0.09$ [6], the discrepancy between the four experimental designs considered here is small, with a difference of around ± 0.003 at 1σ, less than 3% of the best-fit value of a.

In the middle column of Fig. 3, we have computed the sensitivity of the LENF and WBB to the parameter r. Over
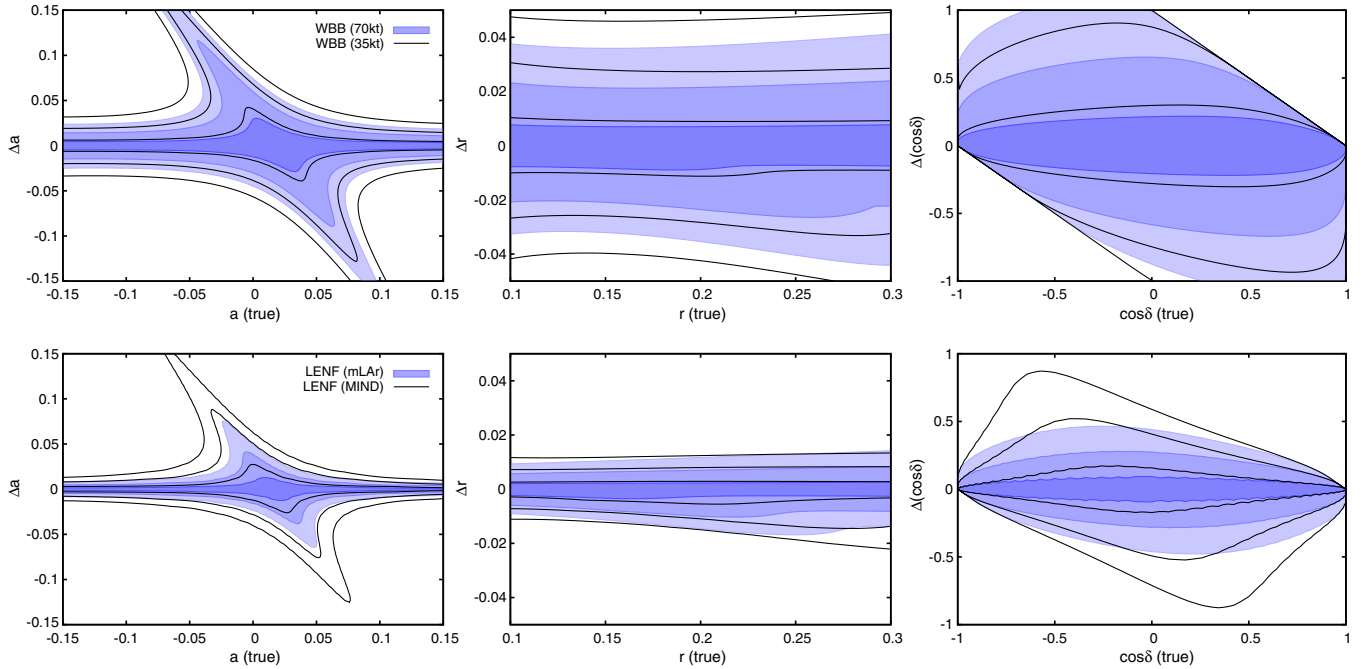
FIG. 3 (color online).   The sensitivity of the next-generation facilities to the a, r and $\cos\delta$ parameters. In all of the plots, the shaded regions progressively show the 1, 3 and 5σ regions for the WBB 70 kton (top row) or the LENF with 50 kton magnetized LAr (bottom row), while the solid lines are the equivalent envelopes for the WBB 35 kton (top row) or the LENF with MIND (bottom row). The leftmost plot shows the sensitivity to a, while the central (rightmost) plot shows the sensitivity to r ($\cos\delta$).

the region of r_{T} that is phenomenologically interesting, this sensitivity is relatively constant at about 0.007 (0.025) for the LENF (WBB) at 3σ. There is a slight broadening of the allowed region towards larger values of r; an effect which is less marked for weaker confidence levels. Once again, we see that LENF uniformly outperforms WBB. The discrepancy is particularly marked at 5σ where the WBB allowed region is around 3.5 times broader than the corresponding region for the LENF. In recent work on the precision of next-generation facilities, it has been shown [32] that only the LENF will be able to surpass the precision on θ_{13} that is expected to be attained by the current generation of reactor experiments. However, the improvement in precision possible with the LENF is rather small, at around 1%, and effectively, the constraints on θ_{13} will be set by the reactor experiments alone [13]. For this reason, the observed discrepancy in precision for r between the LENF and WBB is only expected to influence the ability of the experiments to place individual constraints on sum rules, and should not influence constraints extracted from global analyses of the oscillation data.

The rightmost column of Fig. 3 shows the expected sensitivity to $\cos\delta$ for the LENF and WBB. This measurement has a 3σ precision at its widest point of 0.28 (0.53) for the LENF with magnetized LAr (MIND) and 0.65 (0.89) for the WBB with 35 kton (70 kton) LAr. This decreases dramatically for the extreme points of the spectrum, where the true value of $\cos\delta$ approaches ± 1 and the uncertainty becomes very small for the LENF, while reducing but

remaining sizable at higher significances for WBB. We see that the LENF performs significantly better at this measurement than WBB: at 5σ, even the WBB with 70 kton LAr offers little discriminatory power, with a region that almost covers the whole parameter space, while the LENF offers a reasonable precision which becomes excellent for large values of $|\cos\delta|$. The boundaries of the allowed regions at low significance can be approximated analytically as ellipses: this can be seen by considering a uniform precision on δ itself, $\Delta\delta = \epsilon$, which implies $\Delta(\cos\delta) \equiv \cos\delta_F - \cos\delta_T = -\epsilon\sin\delta_T + \mathcal{O}(\epsilon^2)$. The coordinates $(-\epsilon\sin\delta, \cos\delta)$ provide a parametric description of the ellipse. The assumption of approximately uniform precision in δ is consistent with the simulations performed in Ref. [32] where $\Delta\delta \approx 5° \pm 2°$ for all δ_T. The deviations from ellipticity can be explained by assuming a variable precision on δ as shown in Ref. [32]. Generally, $\cos\delta$ is considerably harder to constrain than r and a. As such, it is expected to introduce a significant uncertainty and should be the dominant limiting factor in the possible constraints on sum rules of the type shown in Eq. (3). However, we must remember that the measurements in this section have focused on a single parameter at a time, and therefore their results cannot be simply combined to understand the precision on a sum rule. Measurements of parameter combinations will in general introduce correlations which may strongly influence the precision, as we will see in the next section.

B. Joint parameter determination

As a first step to understanding the correlations between the measurements of oscillation parameters, we have studied how accurately the parameters a and $\cos\delta$ can be jointly determined for true values which obey a given sum rule. The correlations between the two parameters will show how strongly the true value of one parameter influences the determination of the other. In Fig. 4, we have computed the joint determination of the parameters $\cos\delta_F$ and a_F for a selection of sets of true parameters which obey the sum rule $a_T = r_T \cos\delta_T$, with r_T fixed at its best-fit value derived from global fits of neutrino oscillation data. This simulation uses the LENF with MIND experiment, and incorporates the τ background which is known to impact the attainable precision on a. This plot gives us an indication of the severity of correlations between these two parameters. We see that there is some correlation: the allowed intervals for $\cos\delta$ depend on the true values of a. The width of the allowed regions in both parameters decreases for large absolute values of $|a|$ and $|\cos\delta|$, and this behavior can be understood by comparing it with the results of Sec. VA, where the precision to both a and $\cos\delta$ becomes worse near the origin.

The joint parameter determination plot can give us an indication of how well we can measure the parameters a and $\cos\delta$ if the sum rule is true. In this plot we have assumed that the true parameters obey the sum rule $a = r\cos\delta$ indicated by the dashed line with r set to the best-fit value obtained in the global analysis of neutrino oscillation data, and we have marginalized over all parameters other than a_F and $\cos\delta_F$. The solutions found in the allowed regions are not required to obey the sum rule. For example, although there are plenty of solutions around the origin for $a_T = \cos\delta_T = 0$, the parameter r_F is allowed to vary in the marginalization and can take any reasonable
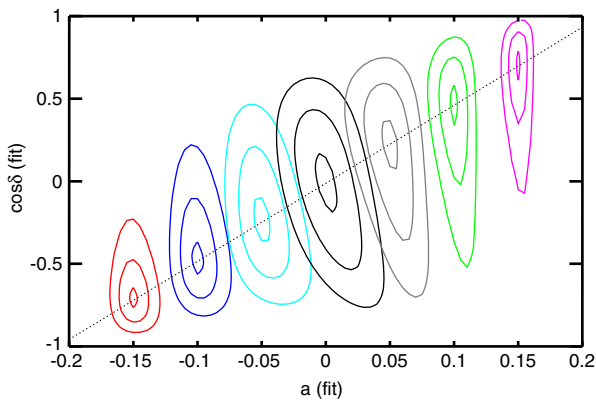

FIG. 4 (color online).   The joint determination of a and $\cos\delta$ for seven sets of true values which obey the relation $a = r\cos\delta$, assuming the LENF with MIND and including τ contamination effects. The dashed line shows the sum rule, and the concentric solid lines indicate the boundary of the 1, 3 and 5σ allowed intervals for the true values of a and $\cos\delta$ at their center.

value, meaning that the final solution rarely satisfies $a = r\cos\delta$. If we are interested in excluding the sum rule without assuming its validity, we must ask a slightly different question: for a general set of true parameter values, which sets of parameters obeying a hypothesized sum rule can be excluded? We will address this question in the next section.

C. Excluding sum rules

The computation of the attainable sensitivity to combinations of oscillation parameters differs from the discussion of the previous section, due to the introduction of nontrivial parameter correlations. In this section, we compute the ability of the LENF and WBB experiments to directly constrain and exclude the sum rules discussed in Sec. IV, while fully incorporating these correlations.

We have scanned over a parameter space spanned by the true value of $\cos\delta$ and the true value of a. At each point in this parameter space, we have found the best fitting set of oscillation parameters which obey a given sum rule, and plotted the corresponding value of $\Delta\chi^2$. Once this value exceeds a chosen significance threshold (for example, 2 and 3σ in Fig. 5), we can consider that sum rule excluded: there are no sets of parameters which obey that sum rule and provide a reasonable fit to the data. When the true parameter set approximately obeys the sum rule in question, we get a good fit, and the width of the surrounding allowed region gives an indication of how sensitive the experiment is to deviations from the sum rule. Technically, this search has been implemented by using a modified form of the $\Delta\chi^2$ statistic. We have extended the $\Delta\chi^2$ to include an additional prior which enforces the sum rule on the set of fitted parameters,

$$\Delta\chi^2 \supset \left(\frac{a_F - a_0 - \lambda r_F \cos\delta_F}{\sigma}\right)^2,$$

where σ is a parameter chosen to be small, ensuring that the sum rule is held to high precision. This term forces the minimal parameter set to obey the sum rule, while not dictating any of the values of the parameters themselves.

We have focused our analysis on the two simplest sum rules $\lambda = 1$ and $\lambda = -\frac{1}{2}$ both with $a_0 = 0$. This is to illustrate the type of constraints that can be placed on parameter correlations in the PMNS matrix, but our approach can be easily generalized to include other types of correlations, beyond the atmospheric sum rules discussed so far. The plots of the left-hand (right-hand) panel on the bottom row of Fig. 5 show the allowed regions for $\lambda = 1$ ($\lambda = -0.5$) for the LENF with magnetized LAr detector (shaded regions) and MIND (contour lines). We see that the largest allowed region, and therefore the hardest point to exclude the sum rule, is when $\cos\delta_T \approx a_T \approx 0$, while the best sensitivity is generally found at large values of $|\cos\delta_T|$. As expected, this behavior is largely inherited
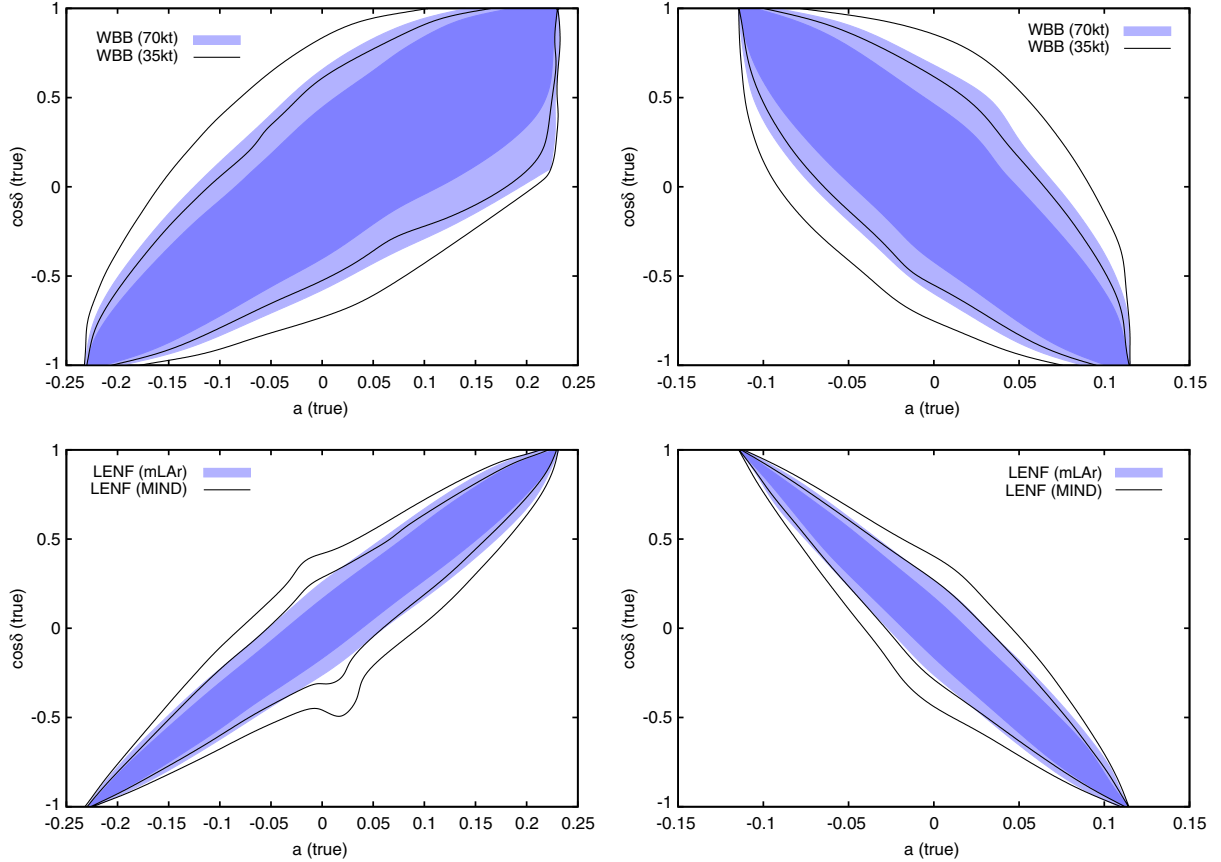
FIG. 5 (color online). The left (right) column shows the ability to exclude models with $\lambda = 1$ ($\lambda = -0.5$) as a function of the true parameters. The plots show the 2 and 3σ allowed regions for the WBB (top row) and the LENF (bottom row). A point lying outside of the contours indicates that the model can be excluded by that given experiment for those true parameter values.

from the sensitivity to $\cos\delta$; however, around the origin we see a novel feature associated with solutions of the type $a = 0$ and $\cos\delta = 0$. For any hypothetical sum rule of the type $a = \lambda r \cos\delta$, a trivial solution can be found for $a_F = \cos\delta_F = 0$. At this point, the ability to constrain both a and $\cos\delta$ is weakened, and we find that regardless of the relationship between the true parameters, provided they are sufficiently close to the origin, we can use this solution to describe the data and satisfy the sum rule. This leads to the lobes around the origin, which are visible particularly for the LENF with MIND (the improved sensitivity to a of the LENF with mLAr mitigates the impact of these solutions). The mLAr detector allows for the sum rule to be excluded over a larger region of parameter space: the 2σ allowed region for the mLAr is contained completely inside the 2σ region for the MIND detector. At the widest points, the allowed regions for $\cos\delta$ cover around 24% (42%) of the parameter space for $\cos\delta$ for the LENF with mLAr (MIND) at 3σ. On the top row of Fig. 5, we show the equivalent regions for the WBB with 35 and 70 kton LAr. These follow the same shape inherited from the uncertainties in measurement of $\cos\delta$. In this case, the uncertainty in $\cos\delta$ is large enough to subsume the lobed

solution regions found for the LENF. The WBB is unable to constrain the parameter $\cos\delta$ to the same extent as the LENF, and we see that the allowed region for the sum rules are correspondingly much larger. At its widest point, the WBB with 70 kton (35 kton) LAr has an allowed region for $\cos\delta$ which covers 56% (81%) of the parameter space at 3σ. For both LENF and WBB, excluding models over even 50% of the parameter space would be an interesting result; however, we have seen that these measurements are challenging, and the more optimistic facilities are required to make significant advances.

D. Constraining λ

Both LENF and WBB will be able to observe violations of a given sum rule for a significant fraction of parameter space, especially if $|\cos\delta|$ is large. In the scenario that the true parameter set appears to agree with some sum rule, it is interesting to see what constraints we can put on the parameters describing such a rule. In this section, we consider the ability of the next-generation oscillation experiments to distinguish between models with similar λ parameters introduced in Eq. (3). Our interest here is in illustrating the
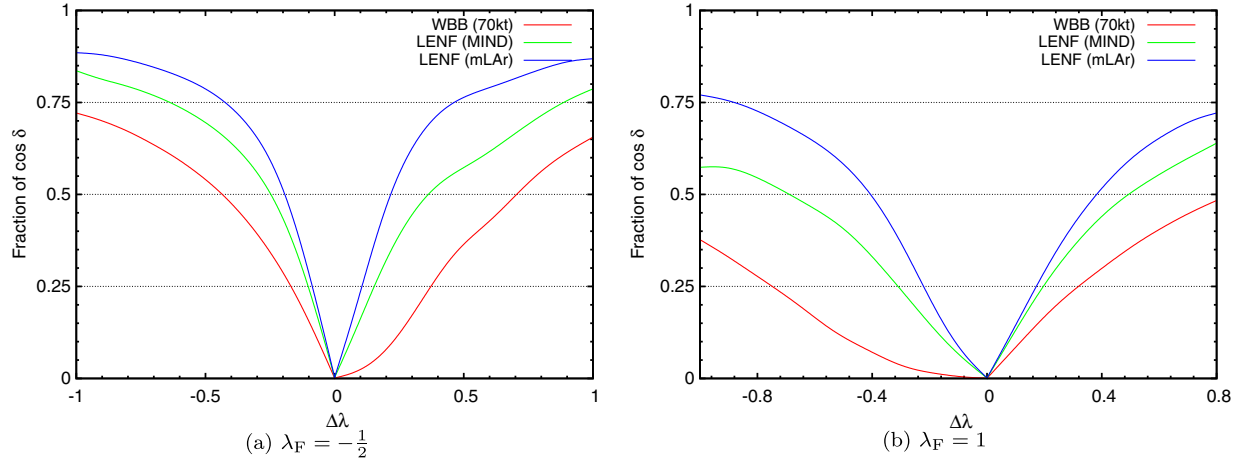
FIG. 6 (color online).   The fraction of values of $\cos \delta_T$ for which the hypothesized value of λ_F can be excluded at 3σ assuming different true values of λ_T. In these plots $\Delta\lambda = \lambda_T - \lambda_F$.

possible constraints that can be posed by a next-generation oscillation experiment, and as such we will restrict our attention to some specific cases; however, the analysis of this section could be simply extended to address other classes of models.

We consider general relations of the type $a = \lambda r \cos \delta$, with continuous ranges of λ in the neighborhoods of the special values $\lambda = 1$ and $\lambda = -1/2$. The plots in Fig. 6 show how well a hypothesized value of λ_F can be excluded as a function of $\Delta\lambda \equiv \lambda_T - \lambda_F$. As the lines of parameters which obey sum rules with $a_0 = 0$ intersect for $\cos \delta_T = 0$, we will always be able to find true parameter values close to this value of $\cos \delta_T$ which satisfy any pair of sum rules. Therefore, it is impossible to distinguish two similar models in all possible cases, and instead we must assess this ability by degree. In order to measure the degree of distinguishability at different facilities, we have plotted a continuous parameter which gives the fraction of values of $\cos \delta_T$ for which we can exclude the hypothesis $\lambda = \lambda_F$ at 3σ. The corresponding fraction of distinguishability for the hypothesis $\lambda_F = -1/2$ ($\lambda_F = 1$) as a function of $\Delta\lambda$ is shown in the left (right) panel of Fig. 6. If we choose our threshold to be 50% of all possible values of $\cos \delta_T$, the LENF with mLAr can distinguish between sum rules of the type $\lambda \approx -1/2$ which deviate by $|\Delta\lambda| \approx 0.2$. If we instead use a MIND, this region increases to $|\Delta\lambda| \approx 0.3$, while the WBB superbeam with a detector of 70 kton is closer to $|\Delta\lambda| \approx 0.7$. For sum rules with $\lambda \approx 1$ the size of these deviations approximately doubles.

For the models presented in Sec. II, which cluster around $\lambda = 1$ or $\lambda = -0.5$, the values of λ differ by around ± 0.1. The ability to separate these candidate models experimentally is clearly dependent on the true value of $\cos \delta$; however, the LENF with mLAr can make this discrimination for about 25% of the values δ at 3σ. This will be a very challenging measurement and is unlikely to be feasible in the next generation of oscillation experiments unless an aggressive strategy is adopted.

VI. CONCLUSIONS

Next-generation neutrino oscillation facilities are not only necessary to resolve the traditional questions about the PMNS matrix, but will also lead the way in a new program of precision neutrino flavor physics. Over the years, many attempts have been made to understand the origin of flavor. One popular approach is to invoke a symmetry to explain the pattern of mixing angles that have been discovered experimentally in the PMNS matrix: an idea which has met with great success and generated a large number of candidate models. Thanks to the precision that is expected at the next-generation oscillation facilities, it will soon be possible to put these theories to the test.

A predictive model of flavor will generally introduce correlations amongst the parameters of the Yukawa sector. The linearized expressions of these correlations are called sum rules, and testing them is a direct way to confirm or exclude a given model. In this paper, we have studied how correlations of the type given in Eq. (3) will be constrained by current and future oscillation experiments. We have seen that, when viewed as predictions for $\cos \delta$, these sum rules are constrained by their consistency with the current data, and although all of the models that we have investigated have some region of applicability, some models may become quite constrained in the near future. The major difficulty in constraining the sum rules found in Sec. II is the absence of information on the parameter $\cos \delta$, and we must look to the next generation of oscillation experiments to provide this. We have studied the ability of two candidate next-generation neutrino oscillation experiments, a low-energy neutrino factory and a wideband superbeam, to constrain these correlations. To illustrate the general constraints

that these experiments can place on flavor effects, we have chosen to focus our attention on sum rules with the form $a = a_0 + \lambda r \cos \delta$, and specifically on the choices $\lambda = 1$ and $\lambda = -0.5$. These have arisen previously in the literature, and we have shown in Sec. II that these two special values appear to well characterize a large class of models. We have seen that violations of these sum rules will be readily testable at the LENF and WBB: the WBB with 70 kton (35 kton) LAr is expected to be able to exclude the relation $a = r \cos \delta$ for at least 44% (19%) of the parameter space, while the LENF with mLAr (MIND) can make the same exclusion for at least 76% (58%). We have also considered the ability to distinguish between models which predict similar sum rules with separations in λ of only around ± 0.1. We have found that this ability is dependent on the exact value of $\cos \delta$; however, it is likely that only the LENF with magnetized LAr is precise enough to make such a distinction at a reasonable statistical significance for 25% of the parameter space.

We have shown that correlations amongst the parameters of the PMNS matrix, as in the atmospheric mixing sum rules considered here, may be tested by the next generation of neutrino oscillation facilities. These correlations can be excluded for a significant part of the parameter space, and constraints can be inferred on the underlying models responsible for them. This not only highlights the important role of the precision neutrino physics program in our search for the origin of flavor, but also the great advances which are possible in the decades to come.

APPENDIX: SUM RULES IN THE HERNANDEZ-SMIRNOV FRAMEWORK

In Ref. [19] a novel approach was developed for the generation of correlations between the parameters of the PMNS matrix following earlier work [49,50]. The method assumes the breaking of a discrete flavor group into two distinct Z_n subgroups which remain unbroken in either the charged lepton or neutrino sector, while broken in the other. Based on this construction, the authors of Ref. [19] reported a number of parameter correlations; however, these correlations led to sum rules identical to those reported in previous studies. In this section, we weaken some of the assumptions made in the derivations of these relations and generate additional correlations with distinct sum rules. We refer the reader to Ref. [19] for a detailed discussion of the method for finding parameter correlations in the "symmetry building" approach, and we will only summarize the steps here, highlighting where we alter the derivation.

The approach in Ref. [19] assumes that the grand flavor group is a von Dyck group, $D(n, m, p)$. These groups are defined by the presentation

$$S^n = T^m = W^p = STW = 1.$$

The generators S and T are assumed to describe residual symmetries of the Majorana neutrino and charged lepton mass terms, respectively, while W is defined to be the inverse of the product ST. The symmetry of the Majorana neutrino mass term is the Klein group $Z_2 \times Z_2$, which fixes n to be given by $n = 2$. Only one of the Z_2 factors originates from the flavor symmetry and is generated by S, while the other one arises accidentally. If the second Z_2 would be embedded in the group as well, another parameter relation would appear, which fixes the mixing angles as it has been discussed in Ref. [49]. The choice of m and p remains free; however, the assumption that the unbroken group is finite restricts these to specific values.[2] Representing each choice by the ordered pair (m, p), the choices which lead to finite groups are exhausted by five special pairs

$$(3, 3), \quad (3, 4), \quad (3, 5), \quad (4, 3), \quad (5, 3),$$

and two infinite sequences

$$(2, N) \quad \text{and} \quad (N, 2) \quad \forall \, N \geq 2.$$

The former are isomorphic to the groups A_4, S_4, A_5, S_4, A_5, respectively. The two infinite sequences lead to dihedral symmetry groups which do not have irreducible triplet representations and are therefore not considered any further.

For a given (m, p), the two generators S and T must be chosen from the symmetries of the leptonic mass terms, assuming that they are residual symmetries following the spontaneous breakdown of G_f. For this to be the case, the generators S and T must have at least one unit

---

[2]See Ref. [51] for further extensions and generalizations of this approach.

eigenvalue. This is necessary for there to exist a VEV alignment that remains invariant under their action. Under the further assumption that the discrete groups are subgroups of SU(3), we find that the symmetry of the diagonalized neutrino mass matrix must be given by either

$$
S_1' = \begin{pmatrix} 1 & 0 & 0 \\ 0 & -1 & 0 \\ 0 & 0 & -1 \end{pmatrix}, \quad S_2' = \begin{pmatrix} -1 & 0 & 0 \\ 0 & 1 & 0 \\ 0 & 0 & -1 \end{pmatrix},
$$

$$
\text{or} \quad S_3' = \begin{pmatrix} -1 & 0 & 0 \\ 0 & -1 & 0 \\ 0 & 0 & 1 \end{pmatrix}.
$$

Similarly, these constraints imply that the symmetry of the diagonalized charged lepton mass matrix is given by one of the three order-m generators

$$
T_e' = \begin{pmatrix} 1 & 0 & 0 \\ 0 & e^{i\frac{2\pi k}{m}} & 0 \\ 0 & 0 & e^{-i\frac{2\pi k}{m}} \end{pmatrix}, \quad T_\mu' = \begin{pmatrix} e^{i\frac{2\pi k}{m}} & 0 & 0 \\ 0 & 1 & 0 \\ 0 & 0 & e^{-i\frac{2\pi k}{m}} \end{pmatrix},
$$

$$
\text{or} \quad T_\tau' = \begin{pmatrix} e^{i\frac{2\pi k}{m}} & 0 & 0 \\ 0 & e^{-i\frac{2\pi k}{m}} & 0 \\ 0 & 0 & 1 \end{pmatrix}.
$$

where $k \in \{n \in Z_m | n \text{ and } m \text{ are coprime}\}$. Working in the basis of diagonal charged leptons, we have $T_\alpha = T_\alpha'$ and $S_i = U_{\text{PMNS}} S_i' U_{\text{PMNS}}^\dagger$.

With a choice of generators $T_\alpha - S_i$, we can construct W

$$
W^{-1} = S_i T_\alpha = U_{\text{PMNS}} S_i' U_{\text{PMNS}}^\dagger T_\alpha.
$$

As in Ref. [19], it is assumed that W has an eigenvalue 1, which can be shown to constrain $\text{Tr}[W]$ to be real. For the three finite von Dyck groups with a three-dimensional irreducible representation, it can be shown by considerations of the group character tables that this is in fact a necessary property. From the group presentation, we see that the remaining eigenvalues must be pth roots of unity, and therefore, we can express

$$
\text{Tr}[W] = 1 + 2\cos\left(\frac{2\pi d}{p}\right) \quad \text{s.t. } d \in Z_p. \tag{A1}
$$

Once we have computed $\text{Tr}[W]$ we have fully specified the constraints on the PMNS matrix. These fix one of the columns of the PMNS matrix, where the column fixed corresponds to the choice of generator S_i, and the order of the rows on the choice of T_α. In general, the constraints are given by

$$
|U_{\beta i}|^2 = |U_{\gamma i}|^2 = \frac{1 - \eta}{2}, \quad |U_{\alpha i}|^2 = \eta,
$$

where $\{\alpha, \beta, \gamma\} = \{e, \mu, \tau\}$, and η is defined by

$$
\eta = \frac{1 + \text{Tr}[W]}{4\sin^2\left(\frac{\pi k}{m}\right)}.
$$

Combined with Eq. (A1), this produces an expression for η in terms of k and d

$$
\eta = \frac{\cos^2\left(\frac{\pi d}{p}\right)}{\sin^2\left(\frac{\pi k}{m}\right)}. \tag{A2}
$$

In Ref. [19] k is fixed so that $k = 1$ and d is not varied systematically. However, by varying these parameters we can find novel parameter correlations and, as we will show, can generate sum rules which have not been previously identified in the literature.

As we have mentioned, the constraints imposed by this method fix the ith column of the PMNS matrix by symmetry alone. The values of the elements of this column are given by the choice of (m, p) and the choice of two integers k and d. Which column is fixed, and the pattern of values that are imposed, is governed by a choice of one of nine possible pairs of generators. Only four of these choices appear interesting phenomenologically: $T_e - S_1$, $T_e - S_2$, $T_\mu - S_2$ and $T_\tau - S_2$.[3] For these cases, the resulting constraints can always be expressed by two relations: The first leads to an exact expression for s as a function of r. The second relation is a sum rule of the type Eq. (3).

For the choice of generators $T_e - S_1$, we find that these relations are

$$
s = \sqrt{3\left(1 - \frac{2\eta}{2 - r^2}\right) - 1}, \quad a = \sqrt{\frac{\eta}{2(1 - \eta)}} r \cos \delta,
$$

and we find similar relations for $T_e - S_2$

$$
s = \sqrt{\frac{6\eta}{2 - r^2} - 1}, \quad a = -\sqrt{\frac{\eta}{2(1 - \eta)}} r \cos \delta.
$$

For $T_\mu - S_2$, we see a nonzero prediction for a at $r = 0$

$$
s = \sqrt{\frac{3(1 - \eta)}{2 - r^2} - 1},
$$

$$
a = \frac{1 - 3\eta}{2(1 + \eta)} - \sqrt{\frac{1 - \eta}{2(1 + \eta)}} r \cos \delta.
$$

This feature is also present for the choice $T_\tau - S_2$,

---

[3]The remaining five pairs $T_\alpha - S_i$ lead to correlations that cannot be reconciled with the current phenomenological data for any choice of (m, p), k and d.

TABLE II. Analytical expressions for the phenomenologically viable sum rules arising in the Hernandez-Smirnov framework for finite von Dyck groups, as described in Table I. In this table, m gives the order of the generator which controls the charge lepton mass matrix, $T_\alpha^m = 1$, and $\phi = (1 + \sqrt{5})/2$ is the golden ratio.

G_f	m	T_α, S_i	s	a_0	λ
A_4	3	T_e, S_2	$\frac{1}{\sqrt{1-r^2/2}} - 1$	0	$-\frac{1}{2}$
	3	T_μ, S_2	$\frac{1}{\sqrt{1-r^2/2}} - 1$	0	$-\frac{1}{2}$
	3	T_τ, S_2	$\frac{1}{\sqrt{1-r^2/2}} - 1$	0	$-\frac{1}{2}$
S_4	3	T_e, S_1	$\sqrt{1 - \frac{2r^2}{2-r^2}} - 1$	0	1
	4	T_μ, S_2	$\sqrt{\frac{3}{2(2-r^2)}} - 1$	$\frac{1}{6}$	$-\sqrt{\frac{1}{6}}$
	4	T_τ, S_2	$\sqrt{\frac{3}{2(2-r^2)}} - 1$	$-\frac{1}{6}$	$-\sqrt{\frac{1}{6}}$
A_5	5	T_e, S_1	$\sqrt{3 + \frac{6}{(3-\phi)(r^2-2)}} - 1$	0	$\frac{\phi}{\sqrt{2}}$
	5	T_e, S_2	$\sqrt{\frac{6}{(2+\phi)(2-r^2)}} - 1$	0	$\frac{1-\phi}{\sqrt{2}}$
	5	T_μ, S_2	$\sqrt{\frac{3\phi}{(2\phi-1)(2-r^2)}} - 1$	$-\frac{5-4\phi}{22}$	$-\sqrt{\frac{3+2\phi}{22}}$
	5	T_τ, S_2	$\sqrt{\frac{3\phi}{(2\phi-1)(2-r^2)}} - 1$	$\frac{5-4\phi}{22}$	$-\sqrt{\frac{3+2\phi}{22}}$

$$s = \sqrt{\frac{3(1-\eta)}{2-r^2}} - 1 ,$$

$$a = -\frac{1-3\eta}{2(1+\eta)} - \sqrt{\frac{1-\eta}{2(1+\eta)}} r \cos\delta.$$

By comparing the predictions of s for all of the choices of (m, p), k and d with the known phenomenological interval, we identify eight viable scenarios which are listed in Table I together with their numerical predictions for s, a_0 and λ. Analytical expressions for each of these eight scenarios can be found in Table II.

[1] F. P. An *et al.* (Daya Bay Collaboration), Phys. Rev. Lett. **108**, 171803 (2012); F. P. An *et al.* (Daya Bay Collaboration), Chin. Phys. C **37**, 011001 (2013).
[2] J. K. Ahn *et al.* (RENO Collaboration), Phys. Rev. Lett. **108**, 191802 (2012).
[3] K. Abe *et al.* (T2K Collaboration), Phys. Rev. Lett. **107**, 041801 (2011); P. Adamson *et al.* (MINOS Collaboration), Phys. Rev. Lett. **107**, 181802 (2011); Y. Abe *et al.* (Double Chooz Collaboration), Phys. Rev. Lett. **108**, 131801 (2012).
[4] M. Apollonio *et al.* (CHOOZ Collaboration), Eur. Phys. J. C **27**, 331 (2003).
[5] J. Beringer *et al.* (Particle Data Group), Phys. Rev. D **86**, 010001 (2012).
[6] M. C. Gonzalez-Garcia, M. Maltoni, J. Salvado, and T. Schwetz, J. High Energy Phys. 12 (**2012**) 123.
[7] D. V. Forero, M. Tortola, and J. W. F. Valle, Phys. Rev. D **86**, 073012 (2012); G. L. Fogli, E. Lisi, A. Marrone, D. Montanino, A. Palazzo, and A. M. Rotunno, Phys. Rev. D **86**, 013012 (2012).
[8] G. Altarelli and F. Feruglio, Rev. Mod. Phys. **82**, 2701 (2010); H. Ishimori, T. Kobayashi, H. Ohki, Y. Shimizu,

H. Okada, and M. Tanimoto, Prog. Theor. Phys. Suppl. **183**, 1 (2010); S. F. King and C. Luhn, Rep. Prog. Phys. **76**, 056201 (2013).
[9] P. F. Harrison, D. H. Perkins, and W. G. Scott, Phys. Lett. B **530**, 167 (2002).
[10] A. Datta, F.-S. Ling, and P. Ramond, Nucl. Phys. **B671**, 383 (2003); Y. Kajiyama, M. Raidal, and A. Strumia, Phys. Rev. D **76**, 117301 (2007).
[11] S. F. King and C. Luhn, J. High Energy Phys. 10 (**2009**) 093.
[12] S. F. King, J. High Energy Phys. 08 (**2005**) 105; I. Masina, Phys. Lett. B **633**, 134 (2006); S. Antusch and S. F. King, Phys. Lett. B **631**, 42 (2005); S. Antusch, P. Huber, S. F. King, and T. Schwetz, J. High Energy Phys. 04 (**2007**) 060.
[13] S.-H. Seo, in RENO-50 Workshop, 2013; Y. Wang, in Lepton-Photon XXVI, 2013.
[14] S. F. King, Phys. Lett. B **659**, 244 (2008).
[15] S. F. King and C. Luhn, J. High Energy Phys. 09 (**2011**) 042.
[16] X.-G. He and A. Zee, Phys. Lett. B **645**, 427 (2007); W. Grimus and L. Lavoura, J. High Energy Phys. 09 (**2008**) 106; Y. Lin, Nucl. Phys. **B824**, 95 (2010).

[17] S. Antusch, S. F. King, C. Luhn, and M. Spinrath, Nucl. Phys. **B856**, 328 (2012).

[18] W. Rodejohann and H. Zhang, Phys. Rev. D **86**, 093008 (2012); I. deM edeiros Varzielas and L. Lavoura, J. Phys. G **40**, 085002 (2013); C. Luhn, Nucl. Phys. **B875**, 80 (2013).

[19] D. Hernandez and A. Y. Smirnov, Phys. Rev. D **86**, 053014 (2012).

[20] C. Lam, Phys. Rev. D **74**, 113004 (2006); C. H. Albright and W. Rodejohann, Eur. Phys. J. C **62**, 599 (2009); C. H. Albright, A. Dueck, and W. Rodejohann, Eur. Phys. J. C **70**, 1099 (2010); X.-G. He and A. Zee, Phys. Rev. D **84**, 053004 (2011).

[21] P. Huber, M. Lindner, T. Schwetz, and W. Winter, J. High Energy Phys. 11 (**2009**) 044.

[22] P. Huber, M. Lindner, and W. Winter, J. High Energy Phys. 05 (**2005**) 020.

[23] B. Richter, arXiv:hep-ph/0008222.

[24] P. Coloma, T. Li, and S. Pascoli, arXiv:1206.4038.

[25] D. Autiero, J. Aysto, A. Badertscher, L. B. Bezrukov, J. Bouchez *et al.*, J. Cosmol. Astropart. Phys. 11 (**2007**) 011; D. Angus *et al.* (LAGUNA Collaboration), arXiv:1001.0077; A. Rubbia, arXiv:1003.1921; A. Rubbia (LAGUNA Collaboration), Acta Phys. Pol. B **41**, 1727 (2010).

[26] S. Geer, Phys. Rev. D **57**, 6989 (1998); A. De Rujula, M. B. Gavela, and P. Hernandez, Nucl. Phys. **B547**, 21 (1999); A. Bandyopadhyay *et al.* (ISS Physics Working Group), Rep. Prog. Phys. **72**, 106201 (2009).

[27] S. Choubey *et al.*, Report No. IDS-NF-020, 2011.

[28] P. Huber, M. Lindner, M. Rolinec, and W. Winter, Phys. Rev. D **74**, 073003 (2006); S. K. Agarwalla, P. Huber, J. Tang, and W. Winter, J. High Energy Phys. 01 (**2011**) 120.

[29] A. D. Bross, M. Ellis, S. Geer, O. Mena, and S. Pascoli, Phys. Rev. D **77**, 093012 (2008).

[30] E. Fernandez Martinez, T. Li, S. Pascoli, and O. Mena, Phys. Rev. D **81**, 073010 (2010).

[31] P. Ballett and S. Pascoli, Phys. Rev. D **86**, 053002 (2012).

[32] P. Coloma, A. Donini, E. Fernandez-Martinez, and P. Hernandez, J. High Energy Phys. 06 (**2012**) 073.

[33] K. Long, in IDS-NF 10 (2013).

[34] P. Coloma, P. Huber, J. Kopp, and W. Winter, Phys. Rev. D **87**, 033004 (2013).

[35] M. Blennow, P. Coloma, A. Donini, and E. Fernandez-Martinez, J. High Energy Phys. 07 (**2013**) 159.

[36] P. Huber, M. Lindner, and W. Winter, Comput. Phys. Commun. **167**, 195 (2005); P. Huber, J. Kopp, M. Lindner, M. Rolinec, and W. Winter, Comput. Phys. Commun. **177**, 432 (2007).

[37] A. Rubbia, J. Phys. Conf. Ser. **171**, 012020 (2009).

[38] A. Longhin, online resource.

[39] A. Longhin, Proc. Sci., ICHEP2010 (**2010**) 325.

[40] A. Dighe, S. Goswami, and S. Ray, Phys. Rev. D **86**, 073001 (2012).

[41] S. Bertolucci, A. Blondel, A. Cervera, A. Donini, M. Dracos *et al.*, arXiv:1208.0512.

[42] F. J. P. Soler (IDS-NF Collaboration), Proc. Sci., EPS-HEP2011 (**2011**) 105.

[43] R. Bayes, in IDS-NF 10 (2013).

[44] D. Indumathi and N. Sinha, Phys. Rev. D **80**, 113012 (2009).

[45] R. Dutta, D. Indumathi, and N. Sinha, Phys. Rev. D **85**, 013003 (2012).

[46] A. Donini, J. J. Gómez Cadenas, and D. Meloni, J. High Energy Phys. 02 (**2011**) 095.

[47] A. Rubbia *et al.*, Report No. CERN-SPSC-2012-021, SPSC-EOI-007, 2012.

[48] V. Barger, D. Marfatia, and K. Whisnant, Phys. Rev. D **65**, 073023 (2002).

[49] C. S. Lam, Phys. Rev. D **78**, 073015 (2008); C. Lam, arXiv:0907.2206.

[50] S.-F. Ge, D. A. Dicus, and W. Repko, Phys. Lett. B **702**, 220 (2011); S.-F. Ge, D. A. Dicus, and W. W. Repko, Phys. Rev. Lett. **108**, 041801 (2012).

[51] D. Hernandez and A. Y. Smirnov, Phys. Rev. D **87**, 053005 (2013); B. Hu, Phys. Rev. D **87**, 033002 (2013); W. Grimus, J. Phys. G **40**, 075008 (2013); C. Lam, arXiv:1301.3121; D. Hernandez and A. Y. Smirnov, Phys. Rev. D **88**, 093007 (2013).